Energy & Environmental Science

Cite this: DOI: 10.1039/c2ee03583a

www.rsc.org/ees

COMMUNICATION

Graphene–sponges as high-performance low-cost anodes for microbial fuel cells†

Xing Xie,[ab] Guihua Yu,[c] Nian Liu,[d] Zhenan Bao,[c] Craig S. Criddle*[a] and Yi Cui*[be]

Received 29th December 2011, Accepted 14th February 2012
DOI: 10.1039/c2ee03583a

A high-performance microbial fuel cell (MFC) anode was constructed from inexpensive materials. Key components were a graphene–sponge (G–S) composite and a stainless-steel (SS) current collector. Anode fabrication is simple, scalable, and environmentally friendly, with low energy inputs. The SS current collector improved electrode conductivity and decreased voltage drop and power loss. The resulting G–S–SS composite electrode appears promising for large-scale applications.

Microbial fuel cells (MFCs) harness the metabolism of exoelectrogens, microorganisms that mediate extracellular electron transfer, to convert chemical energy into electrical energy.[1–3] Unlike chemical fuel cells that recover energy from purified fuels, such as hydrogen, methane, and ethanol, MFCs tap the enzymatic diversity of self-assembled microbial communities to recover energy from complex organic mixtures, such as human excrement,[4] marine sediment,[5,6] and wastewater.[7] First-generation MFCs relied upon small (and expensive) soluble electron shuttles to mediate electron transfer to and from electrodes. Energy output was low.[8–12] Low power production and high capital cost limited MFC's use to small-scale niche applications in which cost was not a major factor, such as spacecraft[4] or robots.[13] Development of mediator-less MFCs opened the door for larger-scale applications.[14–16] By far the largest potential application is wastewater treatment. In the U.S. alone, more than 126 billion litres of domestic wastewater are generated each day.[7] Treatment of this wastewater accounts for ~3% of electrical energy load.[17] Current treatment technology requires an energy input of ~0.6 kW h per m^3, about half of which is electrical energy used for oxygen delivery to aerobic microorganisms.[17] The wastewater itself contains ~2 kW h per m^3 of chemical energy present as organic matter and ammonium.[18] If less energy was used for treatment and more chemical energy recovered, wastewater treatment facilities could become net energy producers.[17]

Following a 2004 demonstration of domestic wastewater treatment,[7] MFCs have received considerable attention, with >2000 papers published to date. These publications address reactor configuration, electrode material science, exoelectrogen screening and characterization, and optimization of operational conditions. Despite these efforts, however, MFCs are still not used for full-scale wastewater treatment due to high capital costs, low coulombic efficiency, and other energy losses.[17,19] Major breakthroughs are needed to make MFC technology competitive with anaerobic processes that recover energy through conversion of organic matter into methane.[17]

The high capital cost of MFCs is due in part to the materials used for electrode fabrication. High-performance, low-cost electrodes are

[a]*Department of Civil and Environmental Engineering, Stanford University, Stanford, California 94305, USA. E-mail: ccriddle@stanford.edu; Tel: +1-650-723-9032*
[b]*Department of Materials Science and Engineering, Stanford University, Stanford, California 94305, USA. E-mail: yicui@stanford.edu; Fax: +1-650-725-4034; Tel: +1-650-723-4613*
[c]*Department of Chemical Engineering, Stanford University, Stanford, California 94305, USA*
[d]*Department of Chemistry, Stanford University, Stanford, California 94305, USA*
[e]*Stanford Institute for Materials and Energy Sciences, SLAC National Accelerator Laboratory, 2575 Sand Hill Road, Menlo Park, California 94305, USA*

† Electronic supplementary information (ESI) available: Experimental details. See DOI: 10.1039/c2ee03583a

Broader context

The largest potential application of microbial fuel cells (MFCs) is wastewater treatment, but major breakthroughs are still needed to make MFC technology competitive with traditional anaerobic processes in terms of capital cost and energy conversion efficiency. Most graphite-based electrodes and some other newly developed composite electrodes are not applicable for large-scale applications. In this report, we describe a new high-performance and low-cost composite electrode: a graphene-coated sponge with a stainless steel current collector (G–S–SS). A MFC equipped with a G–S–SS anode achieved a maximum current density of 1.32 A m^{-2} or 2.69 × 10^3 A m^{-3} and a maximum power density of 1.57 W m^{-2} or 394 W m^{-3}. The capital cost of the G–S is ~$2000 per m^3 or $4 per m^2 for 2 mm thick pieces. Simulations indicate that the voltage drop and power loss of the G–S–SS are acceptable, even for conduction lengths up to metre scale. G–S–SS composite electrodes appear promising for large scale MFC applications.

needed. Currently, the most commonly used anodes are graphite-based electrodes, such as graphite rods,[15] graphite discs,[6] carbon brushes,[20] carbon cloth,[21] and reticulated vitreous carbon.[22] To improve performance, the inert graphite surface is treated chemically or thermally[23–25] or coated with electrically conductive materials, such as conductive polymers,[26–30] carbon nanotubes (CNTs),[31–34] or noble metals.[35] While these modifications have significantly improved performance, graphite-based electrodes are too expensive for large-scale MFC applications, and surface modifications make them more costly. Although a few non-graphite-based anodes are available, most use expensive materials, such as conductive polymers and CNTs,[36,37] or they require complex and energy-consuming synthetic steps, such as electro-spinning and carbonization.[38] Wang *et al.* recently report a low-cost graphite-coated crumb rubber anode, but performance was not comparable to graphite-based anodes.[39]

In previous work, we introduced three-dimensional (3D) anodes prepared by coating macroscale porous substrates, such as textiles and sponges, with single-walled CNTs.[40,41] These electrodes provide an open 3D structure that is electrically conductive and amenable to microbial colonization. Lab-scale MFCs equipped with these 3D anodes achieved higher volumetric power densities and lower energy losses than traditional graphite-based anodes. But while the cost of textiles and sponge is low, CNT coatings are expensive. Even with low CNT loadings (less than 2 g m^{-2} for a 2 mm thick sheet), the overall cost is similar to that of commercial graphite-based electrodes. A possible alternative is graphene. Graphene coatings can potentially create an electrically conductive surface similar to that of CNT-coated materials, but at considerably lower cost. To investigate this possibility, we fabricated graphene–sponge (G–S) composite electrodes using graphene nanosheets and a coating method similar to the one used previously for CNT coatings.[41,42] To compensate for the decreased conductivity of graphene nanosheets *versus* CNTs, we added a stainless-steel (SS) current collector to the G–S, creating a G–S–SS composite anode. The G–S–SS composite enabled high current

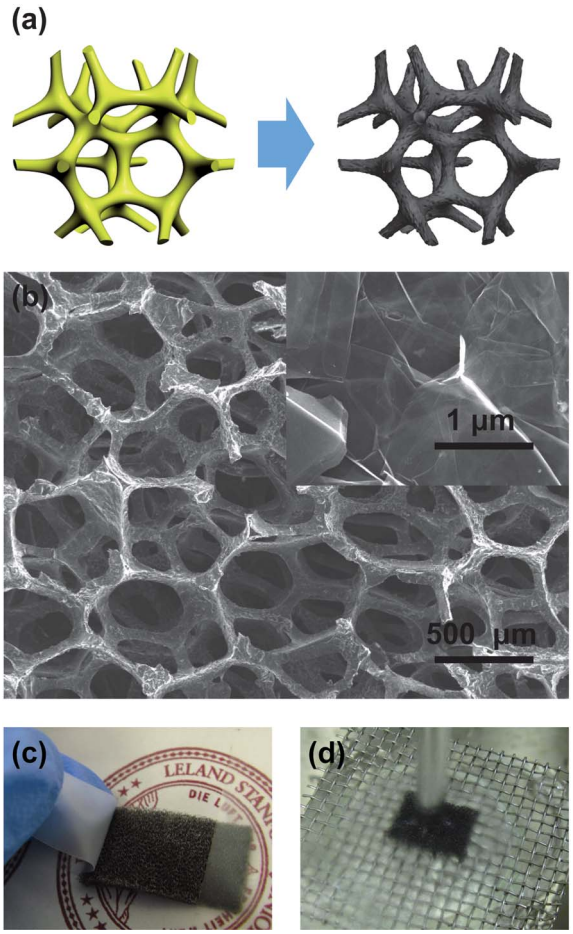

Fig. 1 Graphene–sponge (G–S) composite electrode. (a) Schematic of the plain sponge (left) with three-dimensional (3D) open structure and the G–S composite (right) with conformal graphene coating. (b) Scanning electron microscope (SEM) image of the G–S showing the macroscale porous structure and the graphene surface (inset). (c) Scotch tape test: a piece of Scotch tape was attached to the G–S composite and then peeled off. (d) Water flush: the G–S composite was flushed with water (~100 mL per second) for 10 minutes.

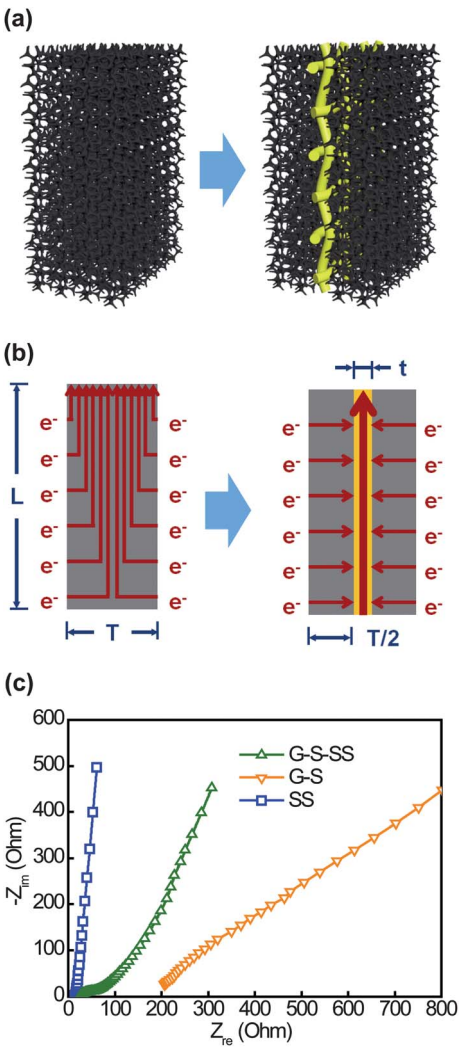

Fig. 2 G–S with a stainless-steel (SS) current collector (G–S–SS). (a) Schematic of the G–S–SS composite electrode (right) *vs.* the G–S composite electrode (left). (b) Schematic showing the electron pathways in the G–S electrode with (right) and without (left) an SS current collector. (c) Nyquist curves of the electrochemical impedance spectroscopy (EIS) tests for different electrodes. The *x*-intercepts on the Nyquist curves are ~14 Ω for SS, ~22 Ω for G–S–SS, and ~180 Ω for G–S, respectively.

density and power outputs in a traditional H-shaped MFC. Theoretical calculations discussed later indicate that this electrode is promising for large-scale applications.

In prior work, we also established the value of sponge electrodes in MFC applications.[41] Living sponges metabolize food and discharge waste while maintaining a continuous flow of water through their porous bodies. The diameters of sponge *ostia* (pores) range from tens to hundreds of microns. This size range provides a balance between the needs for high volumetric throughput of water (*i.e.*, large pores) and high specific surface area (*i.e.*, small pores) for efficient mass transfer of food and nutrients to living cells and for removal of waste.[43,44] Synthetic sponges fabricated from elastomeric polymers are available at low cost and can imitate natural sponges, with pore sizes that are tunable from tens of microns to hundreds of microns.[45] These sponges are ideal for fabrication of 3D electrodes where an open porous structure facilitates electrolyte transport and a high specific surface area facilitates efficient oxidation of organic matter and transfer of electrons to a conductive coating.

To coat sponges with graphene, graphene nano-powder was first dispersed in an aqueous solution by sonication. G–S composites were then fabricated by a simple and scalable dipping-and-drying process that consumes little energy:[46,47] synthetic polyurethane sponges were dipped into the graphene dispersion, removed, and dried at ~90 °C. A schematic of the sponges before and after graphene coating is shown in Fig. 1a. The conductive coating conforms to sponge morphology without changing its open porous structure, as illustrated by scanning electron microscope (SEM) image in Fig. 1b. The flexibility of the 2D feature (Fig. 1b, inset) and strong van der Waals forces enable graphene to wrap the sponge framework conformally and stably.[47,48] A Scotch tape test (Fig. 1c) and a flush with water (Fig. 1d) were carried out to evaluate the durability of the G–S composite. No visible graphene was removed in either experiment (Fig. 1c and Fig S1 in the ESI†). With a graphene loading of ~1 kg m^{-3}, or ~2 g m^{-2} for 2 mm thick pieces, the G–S composite achieved a conductance of ~1 S m^{-1}. Considering that the cost of graphene nano-powder applied in this study is ~$2 per g and the cost of sponge is negligible, the overall price of a G–S composite would be ~$2000 per m^3, or $4 per m^2 for 2 mm thick pieces. This cost is at least one order of magnitude lower than that of the previous CNT coated sponge (CNT–S) composite[41] and of most commercial graphite-based electrodes.[39]

A challenge is that the G–S is about 2 orders of magnitude less conductive than the CNT–S.[41] To address this issue, we used SS meshes as current collectors for the G–S electrodes. A G–S–SS composite electrode was fabricated by gluing a piece of G–S composite to both sides of an SS mesh (Fig. 2a and Fig. S2†). The glue was a conductive carbon paste (Ted Pella, Inc., USA). SS is inexpensive, with a conductance several orders of magnitude greater than G–S, about 10^6 to 10^7 S m^{-1}.[49] We hypothesized that an SS current collector would decrease ohmic resistance by shortening the electron conduction length in the less-conductive G–S, effectively creating an electron transport "highway" (Fig. 2b). To test this hypothesis, we used electrochemical impedance spectroscopy (EIS) to study the ohmic resistance of three electrodes: (1) a G–S electrode (1 cm × 1 cm × 0.4 cm), (2) a G–S–SS electrode (2 pieces of 1 cm × 1 cm × 0.2 cm G–S with an SS mesh current collector in between), and (3) a plain SS mesh (1 cm × 1 cm × 0.05 cm, 20-mesh) electrode (for details, see ESI†). The results are plotted as Nyquist curves in Fig. 2c. The *x*-intercepts (~14 Ω for SS, ~180 Ω for G–S, and ~22 Ω for G–S–SS, respectively) give the ohmic resistance of both the electrode and the electrolyte.[50,51] Because all three electrodes had the same setup and same electrolyte, the decline in resistance from ~180 Ω for G–S to ~22 Ω for the G–S–SS can only be attributed to the SS mesh. This confirms the effectiveness of SS as a current collector.

To test the functionality of G–S–SS electrodes in MFCs, we investigated their use as anodes in a conventional, H-shaped

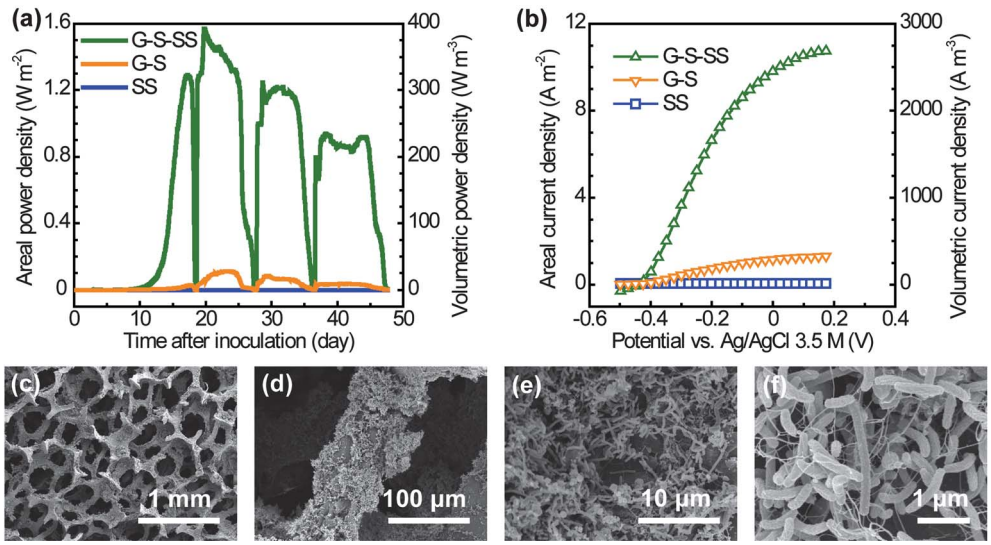

Fig. 3 Characterization of the G–S electrode as an anode for MFCs. (a) Power generation profiles during 50 days of operation, showing that the maximum power density generated by the G–S–SS anode is 14 times that of the G–S anode (1.57 *vs.* 0.111 W m^{-2} or 394 *vs.* 27.7 W m^{-3}). (b) Linear staircase voltammetry (LSV) curves, showing that the maximum current density achieved by the G–S–SS electrode is 8 times that of the G–S electrode (10.7 *vs.* 1.32 A m^{-2} or 2.69 × 10^3 *vs.* 4.23 × 10^2 A m^{-3}). (c–f) SEM images of a colonized G–S–SS anode after 50 days of operation at different scales. Microbial biofilms wrap the branches (d), but do not clog the macroscale pores (c). Most of the G–S anode surface is covered by microorganisms (e) interconnected *via* microbial nanowires (f).

two-chamber MFC. The three different electrodes (G–S–SS, G–S, and SS) were positioned in the same anodic chamber fed with glucose (1 g L^{-1}) and inoculated with anolyte from a previous MFC. The cathode was a carbon cloth electrode coated with Pt catalyst. Power generation profiles are shown in Fig. 3a. The G–S electrode and the G–S–SS electrode both produced power, but the maximum power density of the G–S–SS anode was 14 times that of the G–S anode (1.57 *vs.* 0.111 W m^{-2} or 394 *vs.* 27.7 W m^{-3}). We then used linear staircase voltammetry (LSV) to measure the maximum current densities of the three anodes. As shown in Fig. 3b, the maximum current density of the G–S–SS anode was 8 times that of the G–S anode (10.7 *vs.* 1.32 A m^{-2} or 2.69×10^3 *vs.* 4.23×10^2 A m^{-3}). For the same conditions, the performance of the G–S–SS electrode was comparable to that of CNT-coated electrodes and much better than that of a commercial carbon cloth electrode.[40,41] We also performed EIS measurements on the three electrodes after microbial colonization (Fig. S3†). There was no significant change in the *x*-intercepts of the Nyquist curves, indicating that colonization did not affect conductivity. After 50 days of operation, the anodes were sacrificed for imaging by SEM. Images of the colonized G–S electrode at different scales are shown in Fig. 3c–f and S4†. Microbial biofilms wrapped the sponge branches (Fig. 3d), but did not clog the macroscale pores (Fig. 3c). Most of the G–S surface was covered by microorganisms interconnected by microbial nanowires (Fig. 3e and f), providing a probable direct path for extracellular electron transfer.[52–55] However, the SS control did not enable electricity generation or microbial colonization (Fig. 3a and b). The superior performance of the G–S–SS electrode can therefore be credited to the effects of the SS current collector in decreasing internal resistance.

Some theoretical calculations give insight into the feasibility of a large scale G–S–SS composite. These calculations are based on the following conditions and assumptions: (1) both the G–S composite and the SS mesh are treated as solid materials with conductance values of 1 S m^{-1} and 10^6 S m^{-1}, respectively; (2) the contact resistance between the G–S and the SS is negligible; and (3) the electrode is generating a uniform current density of 10^3 A m^{-3} and the maximum power output is 250 W m^{-3}. As illustrated in the schematic of Fig. 2b, three key variables control voltage drop and the power loss due to internal ohmic resistance: (1) the conduction length (L in Fig. 2b), *i.e.*, the planar dimension of the G–S, (2) G–S thickness (T in Fig. 2b), and (3) the SS thickness (t in Fig. 2b).

Fig. 4a shows the voltage drop and the power loss as a function of conduction length when the G–S thickness is fixed at 4 mm and the SS thickness is fixed at 1 mm. For the G–S electrode, voltage drop and the power loss increase dramatically when the conduction length exceeds 1 cm, indicating that a large-scale G–S electrode would have unacceptable energy losses. In contrast, the voltage drop and the power loss of the G–S–SS electrode are very low (less than 0.006 V and 1.6%, respectively) for a conduction length <1 m. Even at lengths up to 5 m, the voltage drop and power loss are still acceptable (0.05 V and 14%, respectively). These calculations indicate that the use of an SS current collector could dramatically reduce energy losses at large scale.

With a fixed SS thickness of 1 mm, the effects of G–S thickness at different conduction lengths are shown in Fig. 4b. For conduction length within 1 m, the curves almost overlap, indicating that energy losses under these conditions occur within the G–S, and not within the SS current collector. With a G–S thickness of 1 cm, the voltage drop is about 0.03 V and the power lost is about 8%. These numbers climb to 0.11 V and 29% when the G–S thickness is

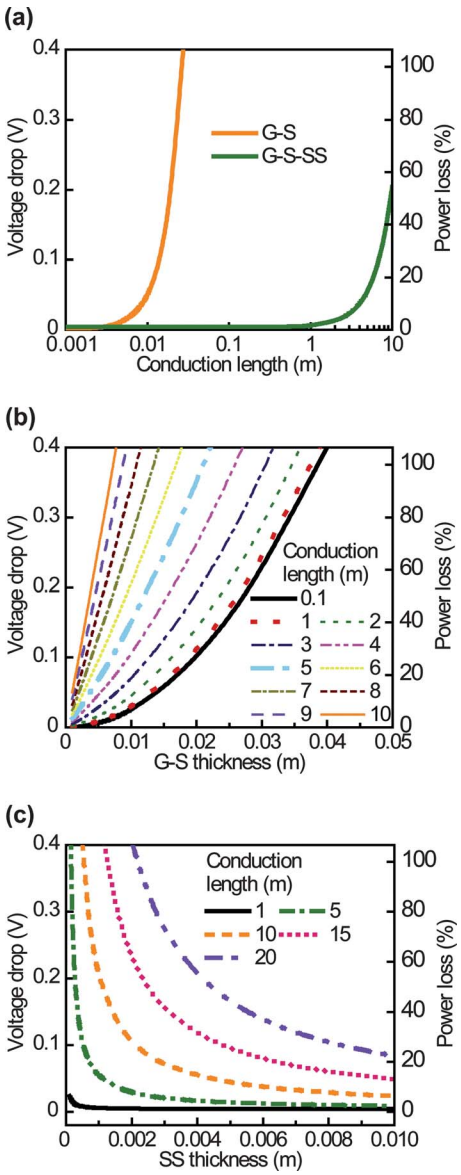

Fig. 4 Simulation results for G–S electrodes in large-scale applications. (a) Voltage drop and power loss for a G–S electrode with and without an SS current collector as a function of electron conduction length, namely the planar dimension. G–S thickness is fixed at 4 mm and the SS thickness is fixed at 1 mm. (b) Voltage drop and power lost for a G–S–SS electrode change with the thickness of the G–S component. The SS thickness is set at 1 mm. The conduction length ranges from 0.1 m to 10 m. (c) Voltage drop and power lost for a G–S–SS electrode change with the thickness of the SS component. The G–S thickness is set at 4 mm. The conduction length ranges from 1 m to 20 m.

increased to 2 cm. Much larger energy losses are observed when conduction lengths exceed 1 m. To prevent voltage drops greater than 0.10 V and power losses exceeding 26%, the maximum G–S thicknesses are 7 mm and 2 mm when conduction lengths are 5 m and 10 m, respectively. The applicable G–S thickness therefore falls within the range of several millimetres to several centimetres, depending upon the conduction length of the G–S–SS. Increasing SS thickness can further improve the conductivity of the G–S–SS composite. Fig. 4c shows voltage drop and power loss at different conduction lengths as a function of SS thickness, when the G–S

thickness is set at 4 mm. When the SS thickness is increased to several millimetres, as expected for practical applications, the voltage drop and the power loss are still acceptable (<0.10 V and <26%, respectively), even at conduction lengths >10 m (Fig. 4c).

In summary, this study demonstrates that low-cost, energy-efficient graphene coated sponge anodes can be produced through a simple fabrication process and that such anodes are amenable to scale-up. The capital cost of the G–S electrode is ~$2000 per m^3, or $4 per m^2 for 2 mm thick pieces, at least one order of magnitude less than most commercial graphite-based electrodes. Laboratory data and theoretical calculations both suggest that an SS current collector effectively improves the conductivity of the G–S electrode thereby reducing voltage drop and power loss. In a lab-scale MFC, the G–S–SS anode achieved a current density and power density comparable to the most effective MFC anodes tested to date. Simulations indicate that the G–S–SS electrode will be effective at conduction lengths of up to metre in scale. The high-performance, low-cost G–S–SS composite clearly holds great promise for field applications, but long-term studies at a large scale are needed.

Acknowledgements

This work was partially supported by the King Abdullah University of Science and Technology (KAUST) Investigator Award (no. KUS-l1-001-12). YC and ZB acknowledge the partial funding support from the Precourt Institute for Energy at Stanford University. XX acknowledges the support from the Stanford Graduate Fellowship and the Stanford Interdisciplinary Graduate Fellowship.

References

1 B. E. Logan, *Nat. Rev. Microbiol.*, 2009, **7**, 375–381.
2 B. E. Rittmann, R. Krajmalnik-Brown and R. U. Halden, *Nat. Rev. Microbiol.*, 2008, **6**, 604–612.
3 D. R. Lovley, *Nat. Rev. Microbiol.*, 2006, **4**, 497–508.
4 J. J. Konikoff, L. W. Reynolds and E. S. Harris, *Aerosp. Med.*, 1963, **34**, 1129–1133.
5 D. R. Bond, D. E. Holmes, L. M. Tender and D. R. Lovley, *Science*, 2002, **295**, 483–485.
6 L. M. Tender, C. E. Reimers, H. A. Stecher, D. E. Holmes, D. R. Bond, D. A. Lowy, K. Pilobello, S. J. Fertig and D. R. Lovley, *Nat. Biotechnol.*, 2002, **20**, 821–825.
7 H. Liu, R. Ramnarayanan and B. E. Logan, *Environ. Sci. Technol.*, 2004, **38**, 2281–2285.
8 K. Tanaka, C. A. Vega and R. Tamamushi, *Bioelectrochem. Bioenerg.*, 1983, **11**, 289–297.
9 G. M. Delaney, H. P. Bennetto, J. R. Mason, S. D. Roller, J. L. Stirling and C. F. Thurston, *J. Chem. Technol. Biotechnol., Biotechnol.*, 1984, **34**, 13–27.
10 S. D. Roller, H. P. Bennetto, G. M. Delaney, J. R. Mason, J. L. Stirling and C. F. Thurston, *J. Chem. Technol. Biotechnol., Biotechnol.*, 1984, **34**, 3–12.
11 R. M. Allen and H. P. Bennetto, *Appl. Biochem. Biotechnol.*, 1993, **39**, 27–40.
12 K. Takayama, T. Kurosaki, T. Ikeda and T. Nagasawa, *J. Electroanal. Chem.*, 1995, **381**, 47–53.
13 S. Wilkinson, *Auton. Rob.*, 2000, **9**, 99–111.
14 H. J. Kim, M. S. Hyun, I. S. Chang and B. H. Kim, *J. Microbiol. Biotechnol.*, 1999, **9**, 365–367.
15 S. K. Chaudhuri and D. R. Lovley, *Nat. Biotechnol.*, 2003, **21**, 1229–1232.
16 F. Scholz and U. Schroder, *Nat. Biotechnol.*, 2003, **21**, 1151–1152.
17 P. L. McCarty, J. Bae and J. Kim, *Environ. Sci. Technol.*, 2011, **45**, 7100–7106.
18 E. S. Heidrich, T. P. Curtis and J. Dolfing, *Environ. Sci. Technol.*, 2011, **45**, 827–832.
19 Y. Qiao, S.-J. Bao and C. M. Li, *Environ. Sci. Technol.*, 2010, **3**, 544–553.
20 B. Logan, S. Cheng, V. Watson and G. Estadt, *Environ. Sci. Technol.*, 2007, **41**, 3341–3346.
21 S. Cheng, H. Liu and B. E. Logan, *Environ. Sci. Technol.*, 2006, **40**, 2426–2432.
22 Z. He, S. D. Minteer and L. T. Angenent, *Environ. Sci. Technol.*, 2005, **39**, 5262–5267.
23 Y. Feng, Q. Yang, X. Wang and B. E. Logan, *J. Power Sources*, 2010, **195**, 1841–1844.
24 S. Cheng and B. E. Logan, *Electrochem. Commun.*, 2007, **9**, 492–496.
25 X. Wang, S. Cheng, Y. Feng, M. D. Merrill, T. Saito and B. E. Logan, *Environ. Sci. Technol.*, 2009, **43**, 6870–6874.
26 M. Adachi, R. Yamamoto, T. Shimomura and A. Miya, *Electrochemistry*, 2010, **78**, 814–816.
27 C. Feng, L. Ma, F. Li, H. Mai, X. Lang and S. Fan, *Biosens. Bioelectron.*, 2010, **25**, 1516–1520.
28 Y. Yuan and S. Kim, *Bull. Korean Chem. Soc.*, 2008, **29**, 168–172.
29 B. Lai, X. Tang, H. Li, Z. Du, X. Liu and Q. Zhang, *Biosens. Bioelectron.*, 2011, **28**, 373–377.
30 Y. Zhao, K. Watanabe, R. Nakamura, S. Mori, H. Liu, K. Ishii and K. Hashimoto, *Chem.–Eur. J.*, 2010, **16**, 4982–4985.
31 H. Y. Tsai, C. C. Wu, C. Y. Lee and E. P. Shih, *J. Power Sources*, 2009, **194**, 199–205.
32 S.-Il. Kim, J.-W. Lee and S.-H. Roh, *J. Nanosci. Nanotechnol.*, 2011, **11**, 1364–1367.
33 Y. Zhao, K. Watanabe and K. Hashimoto, *Phys. Chem. Chem. Phys.*, 2011, **13**, 15016–15021.
34 J.-J. Sun, H.-Z. Zhao, Q.-Z. Yang, J. Song and A. Xue, *Electrochim. Acta*, 2010, **55**, 3041–3047.
35 M. Sun, F. Zhang, Z.-H. Tong, G.-P. Sheng, Y.-Z. Chen, Y. Zhao, Y.-P. Chen, S.-Y. Zhou, G. Liu, Y.-C. Tian and H.-Q. Yu, *Biosens. Bioelectron.*, 2010, **26**, 338–343.
36 Y. Qiao, S.-J. Bao, C. M. Li, X.-Q. Cui, Z.-S. Lu and J. Guo, *ACS Nano*, 2008, **2**, 113–119.
37 Y. Qiao, C. M. Li, S. J. Bao and Q. L. Bao, *J. Power Sources*, 2007, **170**, 79–84.
38 S. Chen, G. He, A. A. Carmona-Martinez, S. Agarwal, A. Greiner, H. Hou and U. Schroeder, *Electrochem. Commun.*, 2011, **13**, 1026–1029.
39 H. Wang, M. Davidson, Y. Zuo and Z. Ren, *J. Power Sources*, 2011, **196**, 5863–5866.
40 X. Xie, L. B. Hu, M. Pasta, G. F. Wells, D. S. Kong, C. S. Criddle and Y. Cui, *Nano Lett.*, 2011, **11**, 291–296.
41 X. Xie, M. Ye, L. Hu, N. Liu, J. R. McDonough, W. Chen, H. N. Alshareef, C. S. Criddle and Y. Cui, *Environ. Sci. Technol.*, 2012, 5265–5270.
42 G. Yu, L. Hu, M. Vosgueritchian, H. Wang, X. Xie, J. R. McDonough, X. Cui, Y. Cui and Z. Bao, *Nano Lett.*, 2011, **11**, 2905–2911.
43 E. E. Ruppert, R. S. Fox and R. D. Barnes, *Invertebrate Zoology: A Functional Evolutionary Approach*, Thomson-Brooks/Cole, 2004.
44 *Sponge Sciences*, ed. Y. Watanabe and N. Fusetani, Springer, 1998.
45 M. Szycher, *Szycher's Handbook of Polyurethanes*, CRC Press LLC, 1999.
46 L. Hu, J. W. Choi, Y. Yang, S. Jeong, F. La Mantia, L.-F. Cui and Y. Cui, *Proc. Natl. Acad. Sci. U. S. A.*, 2009, **106**, 21490–21494.
47 L. Hu, M. Pasta, F. L. Mantia, L. Cui, S. Jeong, H. D. Deshazer, J. W. Choi, S. M. Han and Y. Cui, *Nano Lett.*, 2010, **10**, 708–714.
48 W. Chen, R. B. Rakhi, L. Hu, X. Xie, Y. Cui and H. N. Alshareef, *Nano Lett.*, 2011, **11**, 5165–5172.
49 *Handbook of Chemistry and Physics*, ed. D. R. Lide, CRC Press, 1995.
50 Z. He and F. Mansfeld, *Environ. Sci. Technol.*, 2009, **2**, 215–219.
51 F. Zhao, R. C. T. Slade and J. R. Varcoe, *Chem. Soc. Rev.*, 2009, **38**, 1926–1939.
52 G. Reguera, K. D. McCarthy, T. Mehta, J. S. Nicoll, M. T. Tuominen and D. R. Lovley, *Nature*, 2005, **435**, 1098–1101.
53 N. S. Malvankar, M. Vargas, K. P. Nevin, A. E. Franks, C. Leang, B.-C. Kim, K. Inoue, T. Mester, S. F. Covalla, J. P. Johnson, V. M. Rotello, M. T. Tuominen and D. R. Lovley, *Nat. Nanotechnol.*, 2011, **6**, 573–579.
54 M. Y. El-Naggar, G. Wanger, K. M. Leung, T. D. Yuzvinsky, G. Southam, J. Yang, W. M. Lau, K. H. Nealson and Y. A. Gorby, *Proc. Natl. Acad. Sci. U. S. A.*, 2010, **107**, 18127–18131.
55 Y. A. Gorby, S. Yanina, J. S. McLean, K. M. Rosso, D. Moyles, A. Dohnalkova, T. J. Beveridge, I. S. Chang, B. H. Kim, K. S. Kim, D. E. Culley, S. B. Reed, M. F. Romine, D. A. Saffarini, E. A. Hill, L. Shi, D. A. Elias, D. W. Kennedy, G. Pinchuk, K. Watanabe, S. Ishii, B. Logan, K. H. Nealson and J. K. Fredrickson, *Proc. Natl. Acad. Sci. U. S. A.*, 2006, **103**, 11358–11363.